

# EPIC status of calibration and data analysis

Marcus Kirsch with the inputs from the whole EPIC Consortium  
please send all comments to [mkirsch@xmm.vilspa.esa.es](mailto:mkirsch@xmm.vilspa.esa.es)

This document reflects the status of the calibration of the EPIC camera as implemented in SAS 6.0 with all available CCFs at 30/06/2004. Furthermore the outlook is considered for improvements of calibration which at the moment can be expected for the next SAS release.

## Contents:

<b>1</b>	<b>Calibration Overview</b>	<b>2</b>
1.0	Summary	2
1.1	Imaging	5
1.1.1	Astrometry	5
1.1.2	Point Spread Function and Encircled Energy	6
1.2	Effective Area	10
1.2.1	Mirror collecting area	10
1.2.2	Filter transmission	10
1.2.3	CCD Quantum efficiency	11
1.2.4	Vignetting	12
1.3	Energy Redistribution	14
1.3.1	MOS	14
1.3.2	PN	14
1.4	CTI/Gain	15
1.5	Background	16
1.6	Timing	17
1.7	Examples of EPIC spectra	19
1.7.1	PKS 0558-508	19
1.7.2	PKS 2155-304	20
1.8	Cross Calibration with RGS and other Satellites	21
<b>2</b>	<b>Data Analysis</b>	<b>21</b>
2.1	New features in SAS	21
2.1.1	SAS 5.3.0	21
2.1.2	SAS 5.3.3	21
2.1.3	SAS 5.4.1	21
2.1.4	SAS 6.0.0	22
2.2	Data Analysis	22
2.2.1	MOS	22
2.2.2	PN	23

# 1 Calibration Overview

This section gives a short overview of the status of the calibration of the EPIC instruments MOS1, MOS2 and PN, operating on-board the XMM-Newton observatory. It summarises the quality of the calibration to the extent that this may influence the scientific interpretation of the results.

The instrument calibration is based on a physical model of the various components including mirror response, filter transmission and detector response (energy redistribution, gain, CTI). During ground calibration various components were calibrated and the physical model for each component was optimised. These models were verified in flight and are, where relevant, continuously monitored (e.g. contamination of the detector, changes in gain and CTI due to radiation damage). Where applicable, corrections which are needed for these time-variable changes will be applied to the Current Calibration Files (CCFs) and/or the processing software.

For more detailed information see the release notes of the CCFs at: <http://xmm.vilspa.esa.es/ccf/releasenotes/>

Blue coloured text gives distilled information or html links. Red coloured text marks current problems.

## 1.0 Summary

We give in the next table a summary of the status of the calibration:

Effect	Max. Error	Energy dependent	Off axis angle dependent
Absolute Astrometry	1''(r.m.s.)	NO	YES
Relative Astr. within 1 camera	1.5''(r.m.s)	NO	YES
Relative Astr. between 2 cameras	1.5''(r.m.s)	NO	YES
Point Spread Function	2 %	YES	YES
Relative Effective Area	± 5 %	YES	YES
Absolute Effective Area	± 10 %	YES	YES
Absolute Energy scale	± 10 eV	YES	YES
Relative Timing	$\Delta P/P < 1E-8$	NO	NO
Absolute Timing	250-500 $\mu s$	NO	NO

### Improvements since the 2.1 issue of that document:

- Vignetting and Boresight:** One of the most important outstanding problems of the calibration is a possible offset of around 1' in the telescope axis from nominal. This does not affect the astrometry but could be the reason for flux discrepancies between MOS and PN caused by the vignetting correction which has not yet been adapted to this offset. The offset was determined and implemented in the corresponding CCF (XMM\_MISCDATA\_0020). The new consideration of the right optical axis position improves the vignetting correction, such that it is now applied for correct off axis angles, that could not be calculated correctly before due to the wrong information for the optical axis. This improves differences in flux for off axis sources for each camera from  $\pm 14\%$  to  $\pm 5\%$ . Detailed information at: (see: XMM-SOC-CAL-SRN-156).

The new optical axis position required also a new XMM\_BORESIGHT CCF which holds for each instrument a triple of three angles describing the alignment of the respective instrument boresight with respect to the satellite

coordinate frame. Using the OMC2/3 field new boresight alignment angles for all the three cameras have been calculated.

In a further analysis the XMM\_BORESIGHT CCF in combination with the MOS LINCORDD CCFs has been refined in order to improve the astrometry. (see XMM-SOC-CAL-SRN-168 and XMM-SOC-CAL-SRN-166)

- **PSF:** New analysis has refined the values stored in the King function parameterisation of the 3 EPIC telescope point spread functions (PSFs), i.e. XRT1, XRT2 and XRT3. They are stored in the KING\_PARAMS extension of the CCF, and are tabulated as functions of ENERGY and THETA (off-axis angle). The linear dependencies of the PSF core radius  $r_0$  and slope  $\alpha$  with energy, obtained through earlier studies, have been found to be incorrect; in actuality, the  $r_0$  and  $\alpha$  curves are seen to be initially much flatter with energy, at least out to  $\sim 8$ -10 keV, where they then become rapidly steeper. Usage of the new PSFs yields consistent spectral fits for various different annular extraction regions such as they are used in the analysis of piled-up sources. A consequence of improvements to the model of the PSF is that, in the case of piled-up point sources, excising the piled-up core is now considered to be a valid analytical strategy. Users should use the *epatplot* SAS package to assess the presence and level of pile-up (see: XMM-SOC-CAL-SRN-0167).
- **MOS Low Energy:** Observations of calibration targets confirm a significant change in the low energy redistribution characteristics of the MOS cameras with time. This change is probably due to an increase in the surface charge loss property of the CCDs which degrades the low energy resolution. Epoch dependent calibration files have been produced which reflect these changes, but users should be aware that uncertainties in the model of the redistribution function of the MOS cameras remain. Spectral fitting can be performed down to 150 eV, but in these cases it is recommended that an error term of 2-5% on the model be added in quadrature to that on the data, for example via the "systematic" command within XSPEC (see: XMM-SOC-CAL-SRN-169). Following this recipe the calculated error on spectral parameters such as column density will be more representative of the current uncertainties in the low energy calibration. Note however that the absolute flux calibration in the energy range below 500 eV between the MOS and the pn cameras can differ by up to 20 %. Further work is being carried out on both the MOS and pn calibration to resolve this difference.
- **MOS Gain:** An improvement in the epoch dependent CTI and Gain correction in SAS 6.0.0 has reduced the uncertainty in the energy calibration from 10 to 5 eV for the imaging modes of the MOS cameras. (see: XMM-SOC-CAL-SRN-161).
- **MOS CTI:** For MOS-Timing mode the CTI correction was changed improving earlier over correction by debugging some erroneous code in SAS. MOS Timing mode energy accuracy does now agree with the imaging modes within 0.3 %. (source code change in SAS 6.0).

### Important ongoing calibration topics:

- **PN CTI:** The EPIC pn Small Window mode currently shows a Gain/CTI under correction of  $\sim 2$ -3 % most prominent around the O-edge. This can lead to residuals in the fitted spectra of up to 20 %. A better CTI correction will be provided as soon as possible with a new CTI CCF release. The internal calibration source shows an over correction of up to 15 eV at Mn-K in pn Extended Full Frame mode, that is related to imperfect Gain/CTI correction. This is currently under investigation with special calibration observations.
- **PN redistribution:**
  - EPIC-pn spectra from zeta Puppis have shown that the spectral response below about 400 eV might not yet be correctly reproduced. In particular the re-distribution as modelled in SAS 6.0.0 might be higher than seen in the data. This can lead to large (30%) systematic errors in the absolute flux of very soft spectral components ( $kT < 100$  eV). Further observations with different read-out modes are planned to investigate the problem.
  - EPIC-pn spectra show an excess below 500-1000 eV of about 20 % in SW mode. Current investigations point in the direction of a redistribution problem above the O-edge. On-going work on the pn redistribution is expected to bring down the discrepancy below 10%.
- **EPIC-MOS** cameras show for energies above 3keV an **excess** up to 15 % with respect to EPIC-pn that might be related to various system components and is under investigation.

- **PSF core:** The improved King function of the PSF is a good but not perfect fit to the PSF of the telescopes, as the core of the PSF is very slightly underestimated. This effects the MOS more than the pn (as the MOS detector pixels are much smaller than the pn pixels). This can produce an error in the enclosed energy of at most ~2 %, depending on instrument, energy and extraction radius. Work is currently underway to model the PSF as a combination of a King function plus a Gaussian function (the latter to model the slight excess at the core).
- **Astrometry:** A possible residual in the position angle rotation (Euler  $\psi$  angle) of the order of 0.1 deg are under investigation. This could lead to an uncertainty of up to 1.5'' at the edge of the XMM-Newton field of view.

## 1.1 Imaging

### 1.1.1 Astrometry

Astrometry means: The precision with which astronomical coordinates can be assigned to source images in the EPIC focal plane. We distinguish between: Absolute Astrometry (relative to optical coordinates, without taking into account possible shifts due to spacecraft miss-pointing), Relative Astrometry per camera (within one camera after applying possible shifts due to spacecraft miss-pointing) and Relative Astrometry between cameras (positions in one camera relative to an other one)

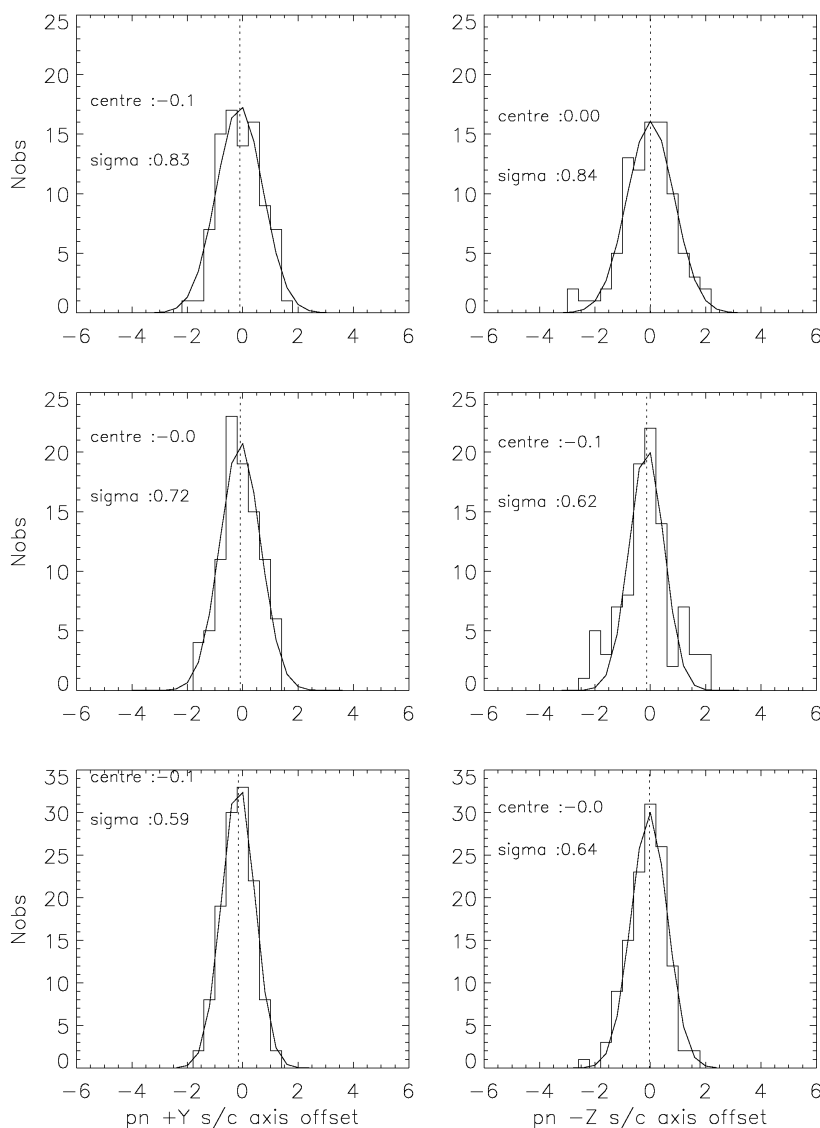


**Figure 1-1:**

**Histogram of the distribution of offsets for each EPIC camera with respect to the 2MASS reference frame projected on to the two spacecraft axis. Top: MOS1, Middle: MOS2, Lower: pn (Details at XMM-SOC-CAL-SRN-168)**

The XMM-Newton absolute astrometry accuracy is limited by the precision of the Attitude Measurement System. Fig. 1-1 shows that the shift from the XMM-Newton-EPIC to the optical frame is on average 0'' with a standard deviation of less than 0.8'' per axis. Hence the [Absolute Pointing Accuracy](#) is considered to be better than 1'' (r.m.s.).

The [relative astrometry within each camera](#) is accurate to 1.5'' for all cameras and over the full field of view. The MOS metrology has been revised with SAS6.0, searching for systematics in the offsets of MOS peripheral CCDs with respect to the central CCD by using observations on rich stellar fields. CCD offsets of up to 2.7'' have been corrected in the MOS LINCORD CCF issue 17. With this new CCF the MOS relative astrometry accuracy has been assessed to be 1.5'' (r.m.s.) while it is as good as ~1.0'' (r.m.s.) for EPIC-pn.

[Among all three EPIC cameras the relative astrometry is also estimated to be better than 1.5'' across the whole field of view.](#)

Note that for faint MOS sources near the detection limit the statistical accuracy of the measurement limits the 90 % confidence contours to 2-4''.

[A possible residual in the position angle rotation \(Euler  \$\psi\$  angle\) of the order of 0.1 deg is under investigation. This could lead to an uncertainty of up to 1.5'' at the XMM-Newton field of view.](#)

### 1.1.2 Point Spread Function and Encircled Energy

**Point Spread Function:** The spatial distribution of light in the focal plane in response to an observed (monochromatic) point source. The PSF integrates to 1 over the infinite focal plane.

**Encircled Energy:** The fraction of the energy of a point source collected within a certain radius.

Though the shape of the PSF is quite complex, the radially averaged profile can be adequately represented by an analytic function - a King function - whose parameters, core radius  $r_0$  and index  $\alpha$ , are themselves functions of energy and off-axis angle:

$$PSF = A \left[ 1 + \left( \frac{r}{r_0} \right)^2 \right]^{-\alpha}$$

It is worth noting that both this function and its integral are analytic.

Earlier work (EPIC-MCT-TN-011, EPIC-MCT-TN-012, XMM-CCF-REL-116) used many bright point sources both on and off axis to determine the energy dependent PSF. This resulted in a linear dependency of  $r_0$  and  $\alpha$  with energy and off-axis angle. It is shown in XMM-SOC-CAL-SRN-0167 that this linear dependency is not valid - the dependencies of  $r_0$  and  $\alpha$  are seen to be flatter (almost constant) with energy (at least out to ~ 8-10 keV). Thereafter the dependencies rapidly turn steeper.

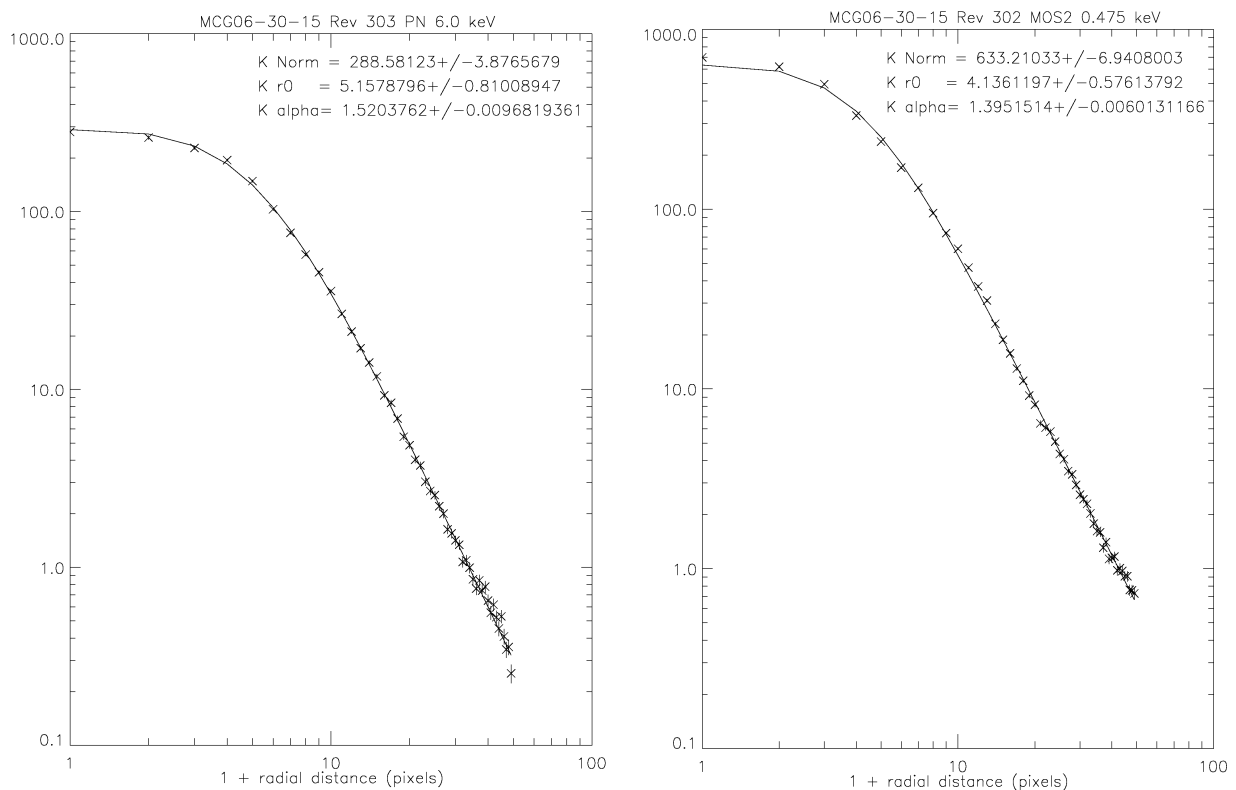
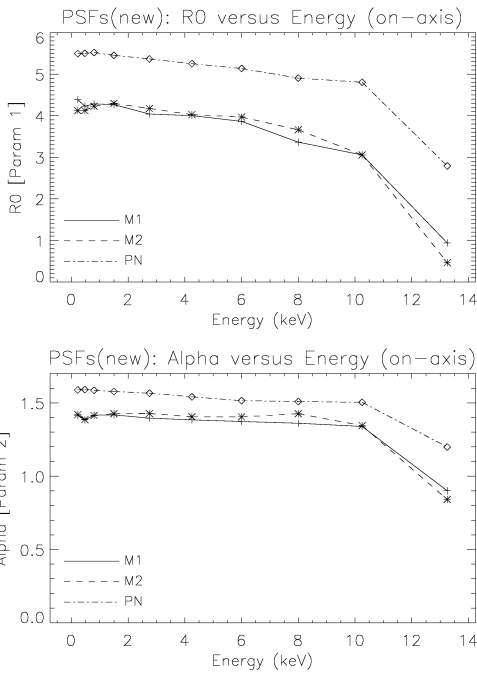


**Figure 1-2: Surface brightness radial profiles (crosses) plus fitted King profiles (lines) for two examples: (left) MCG-06-30-15 Rev. 303 pn at 6 keV (right) MCG-06-30-15 Rev. 302 MOS2 at 0.475 keV.**

Two threads of analysis using data from very long and clean Small Window mode observations of very bright non piled-up sources were followed: One involved the forming of narrow-energy-band images, and fitting the surface brightness radial profiles obtained from these images with a King function to obtain  $r_0$  and  $\alpha$  as a function of energy. A second analysis thread involved the extraction of spectra from narrow annuli around point sources, and once ARF files had been

generated (this involving the actual form of the PSF), the spectra were fitted with standard spectral models, to see how (if at all) the spectral parameters obtained varied with extraction radius.



This whole process was repeated for several sets of PSF parameters (including those obtained from the surface brightness radial profile fitting described above). Two examples of surface brightness radial profiles plus fitted King profiles are shown in Fig.1-2.

The resultant dependencies of  $r_0$  and  $\alpha$  are seen to be flatter (almost ~constant) with energy, at least up to ~8-10 keV (where the  $r_0$  and  $\alpha$  relationships turn over) than in the previous parameterisation of the PSFs as shown in Fig. 1-3.

The new PSFs were used in the analysis of spectra extracted from narrow annuli around a number of bright point sources, as described above. Fig. 1-4 shows how the fitted normalization and power-law index vary as a function of the radial distance of the extraction region (0-5", 5-10" etc.) for the old CCF PSFs and the new CCF PSFs described here, for the MCG-06-30-15 Rev.302 data. A point source, of course, should show no variation in fitted spectral parameter whether the spectrum is extracted from the very centre of the distribution or from the wings, but usage of previous PSFs result in a very wide range in spectral parameters for different radii. Usage of the new PSFs gives rise to a very significantly improved situation, with the fitted normalization and power-law index remaining constant and 'flat' with radius.

**Figure 1-3:  $r_0$  – Energy (top) and  $\alpha$  – Energy (bottom)dependencies for the MOS1, MOS2 and pn on-axis PSFs.**

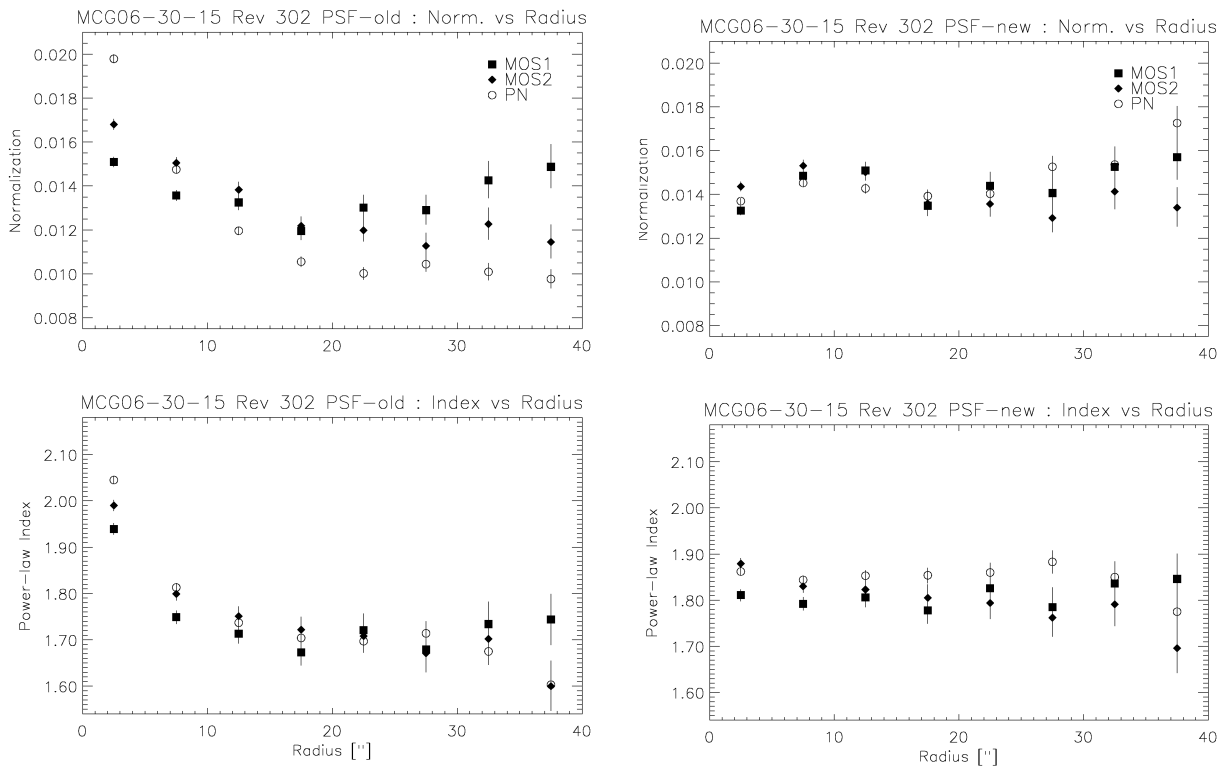


**Figure 1-4: Plots showing how the fitted normalization (top) and power-law index (bottom) vary as a function of the radial distance of the extraction region (left to right: 0-5" (circle), 5-10" (annulus) etc), using the current CCF PSFs (left) and the new CCF PSFs (right) for the MCG-06-30-15 Rev. 302 data.**

A major problem with the previous parameterisation was its inability to produce consistent spectral fits for annular extraction regions such as those for instance used for the analysis of piled-up sources. Hence MCG-6-30-15 (from Rev 302) has been extracted from annuli of 5-40", 10-50" and 15-60" and fits compared to those of a circular extraction (0-30"). This has been performed using the old and the new PSFs, and the results are presented in Fig. 1-5. Whereas usage of the old PSFs results in a per instrument normalization variation of up to 40%, and changes in the fitted spectral slope of 0.2, the **new PSFs give rise to normalization variations of nearer 5% and a spectral slope change of at most 0.03**.

Note that the King function is a good but not perfect fit to the PSF of the telescopes, as **the core of the PSF is very**

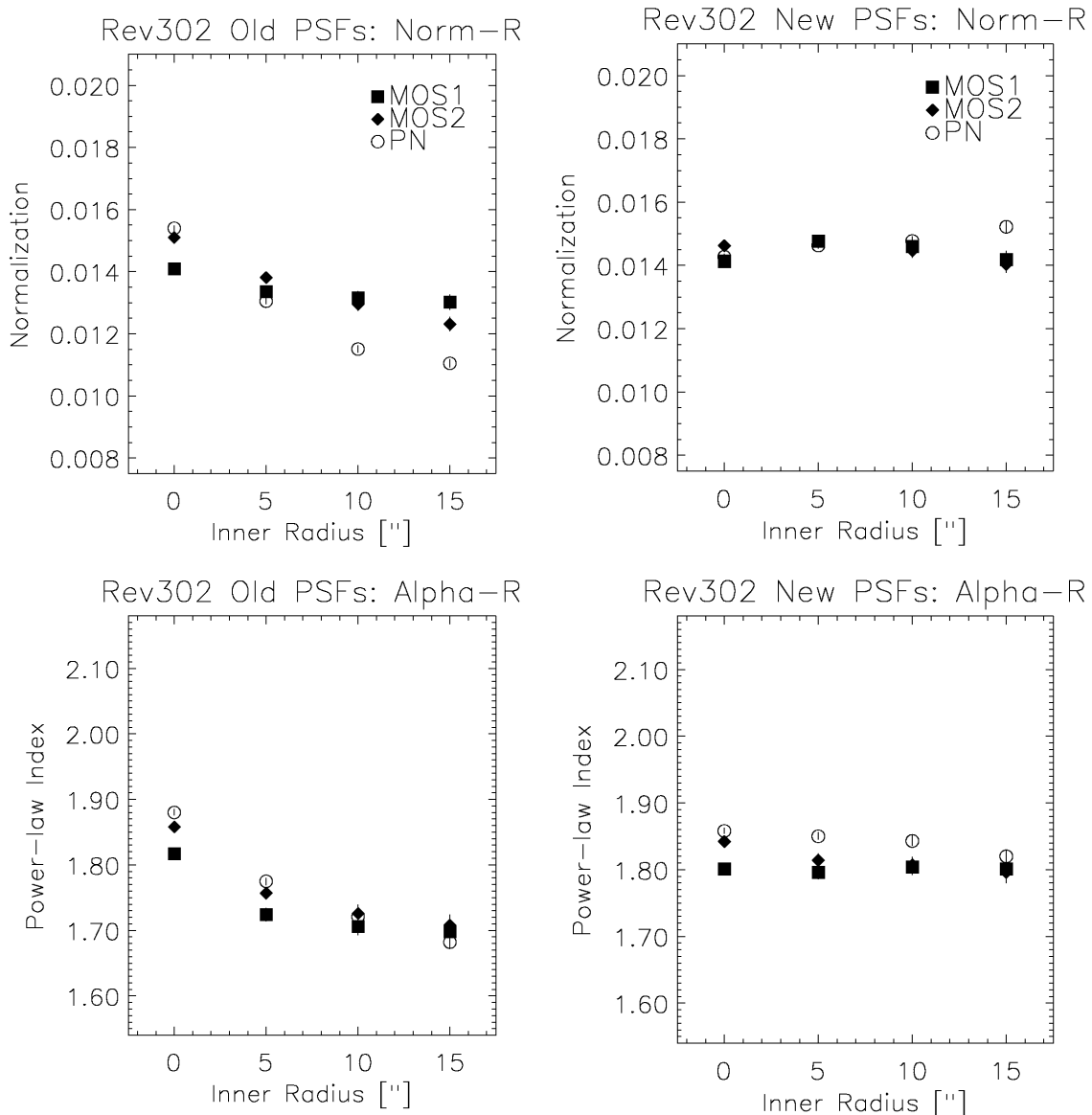


**Figure 1-5: Plots showing how the fitted normalization (top) and power-law index (bottom) vary as a function of extraction region (left to right: 0-30" circle, 5-40" annulus, 10-50" annulus, 15-60" annulus), using the old CCF PSFs (left) and the new CCF PSFs (right) for the MCG-06-30-15 Rev.302 data.**

**slightly underestimated. This effects the MOS more than the pn** (as the MOS detector pixels are much smaller than the pn pixels), and can be seen in Fig. 1-2, the MOS PSF (right) fit lying underneath the data points at the very centre. **This can produce an error in the enclosed energy of at most ~2 %**, depending on instrument, energy and extraction radius. Work is currently underway to model the PSF as a combination of a King function plus a Gaussian function (the latter to model the slight excess at the core).

### Off-axis PSF

As yet, no sources bright enough for this new type of analysis to be performed off-axis have been observed. As such, the general off-axis results of previous work (EPIC-MCT-TN-011, EPIC-MCT-TN-012, XMM-CCF-REL-116) have been used to transform the new on-axis parameters presented here to projected off-axis values.

How the PSF varies off-axis is only known reasonably well for small off-axis values. The following two plots show the details for the reliability:

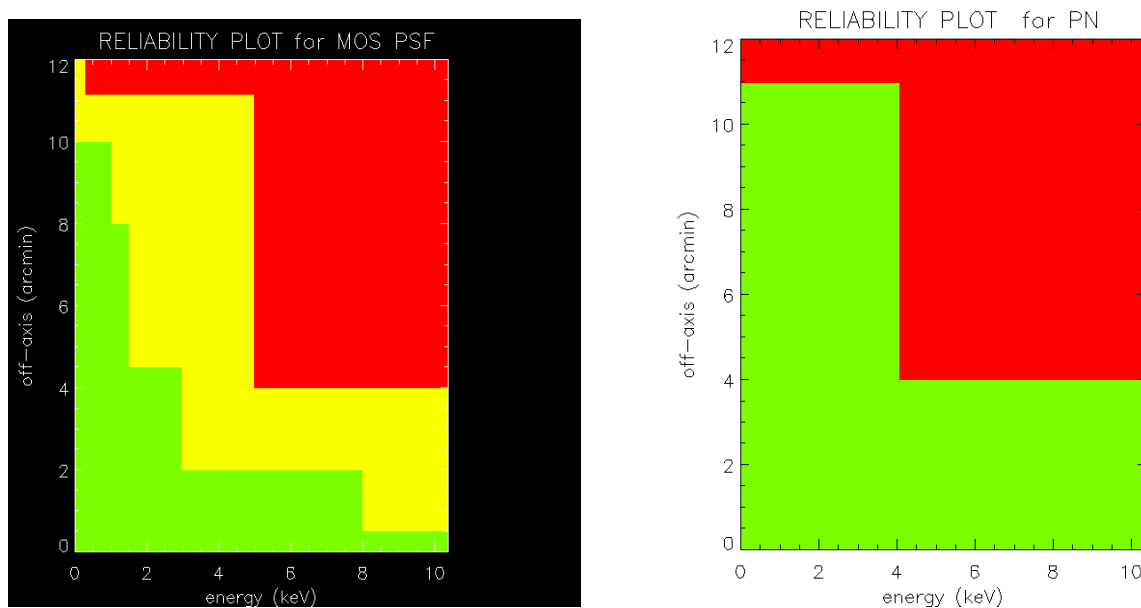


**Figure 1-6: Reliability for PSF**

In the **green region**: For low energies and nearly on-axis positions a large quantity of data is available and in general statistics for these measurements is good. Error bars are in general small ( $\sigma/r_0$  (or  $\alpha$ )  $\sim 1\%$ ) and the  $r_0$  and  $\alpha$  evaluations for these curves are not very "far" from the final fit ( $\Delta r/r < 5\%$  is the worst case).

In the **yellow regions**: for some off-axis angles few measurements are available ( $< 2-3$ ) at the different energies. In general these measurements have large errors ( $\sigma/r_0 \sim 10\%$ ) and the  $r_0$  and  $\alpha$  parameters for these sources sometimes are "far" from the final best-fit values ( $\Delta r/r$  can be as large as 10-20%).

In the **red region**: no calibration data are available, and best-fit values coming from the model are an extrapolation, not a real calibration.

### Addendum: Off-axis PSF

While the EPIC-pn PSF is azimuthally symmetric, the placing of the CCDs in the MOS cameras to follow the focal plane results in a **chip-to-chip variation in the MOS PSF** (ref Saxton, R.D., Denby, M., Griffiths, R.G., Neumann, D.M., 2003, Astron.Nach., 324, 138.). This is **not currently modelled in the SAS** calibration but will result in an azimuthal variation in the encircled energy fraction which is dependent on the extraction radius and the off-axis angle. This variation is not yet quantified but is estimated to be  $\pm 4\%$  for a source circle of radius  $25''$  at an off-axis angle of  $7'$ .

## 1.2 Effective Area

Effective Area means: the effective collecting area of the optical elements and detector system of the EPIC cameras as a function of energy.

For on-axis sources an internal accuracy of **better than 5%** in the determination of the total effective area is reached over the spectral range **from 0.4 - 12 keV** for each instrument separately.

The **cross calibration between MOS1 and MOS2 agrees within 5 %**.

The **MOS/PN cross calibration agrees to 10 % from 0.4 keV to 12 keV**. In the range **from 0.3-1.0 keV the PN camera shows a up to 10 % higher flux than the MOS**, while **for energies above 1.5 keV the MOS flux is up to 10 % higher than the PN (see 1.7.2)**. This is currently under intens investigation and could be due to uncertainties in the vignetting and CCD-Quantum-Efficiency.

### 1.2.1 Mirror collecting area

Mirror collecting area means: the face-on area of the mirror system that reflects X-rays to the focal region

The mirror collecting area has been measured on ground and verified in orbit.

### 1.2.2 Filter transmission

Filter transmission means: the fraction of X-ray photons that through pass the filter

The filter transmission has been measured on ground. The following plot shows filter transmission curves for all the cameras.

For the thick filter the green curve shows the single transmission function currently used in the CCFs for MOS1, MOS2 and PN. Later the CCFs will be refined to reflect the small differences among the three thick filters.

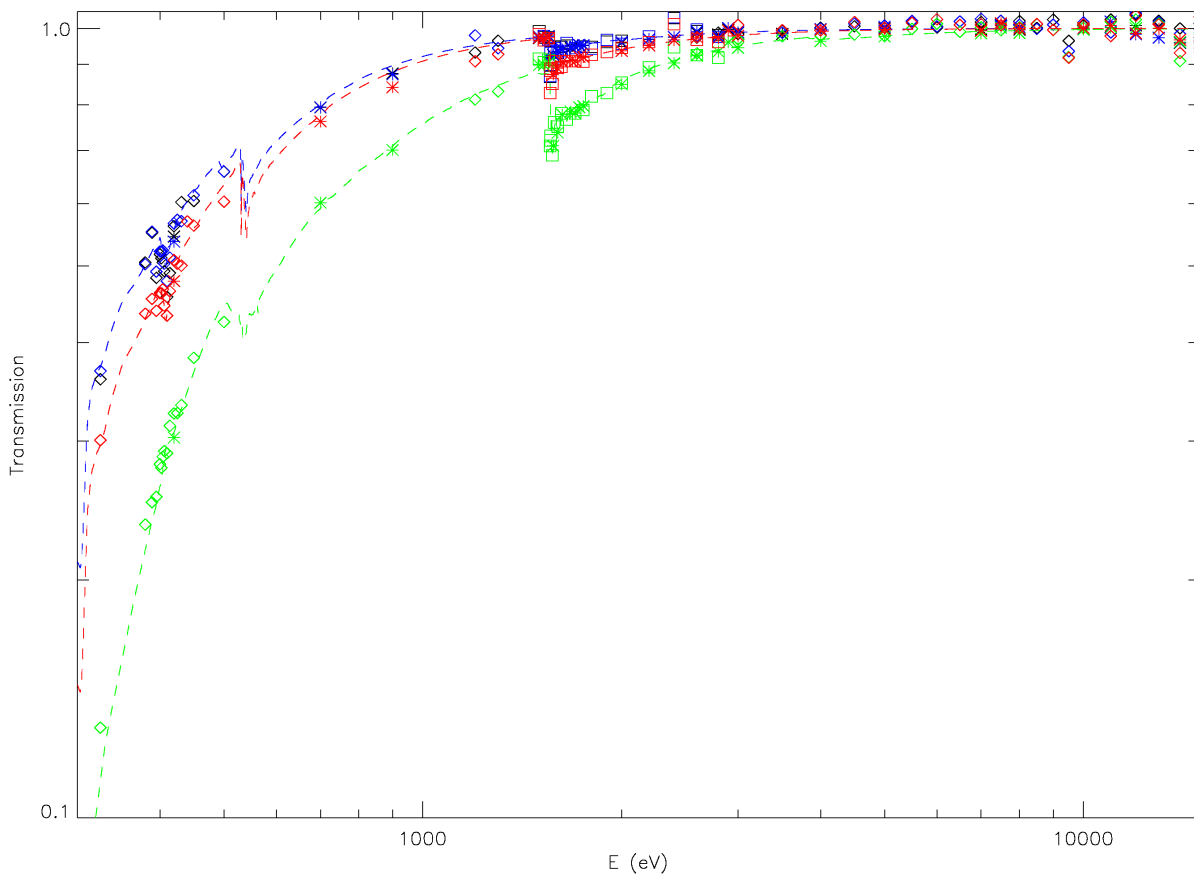


**Figure 1-7: Filter transmissions in CCF and ground calibration filter measurement data points.**  
green - thick, red - medium, blue- thin (Thin1 & Thin2 have the same CCF)  
ground: squares-PN, star-M1, diamond M2 , CCF: dashed lines

### 1.2.3 CCD Quantum efficiency

Quantum Efficiency means: the fraction of photons that generate an event in the CCD.

Ground calibration measurements have shown that the quantum efficiency of MOS CCDs is spatially uniform above 400 eV. Below this energy spatial variations within a CCD are seen as patches in the outer parts of the CCDs where the response is degraded. This inhomogeneity is currently not taken into account by the SAS.

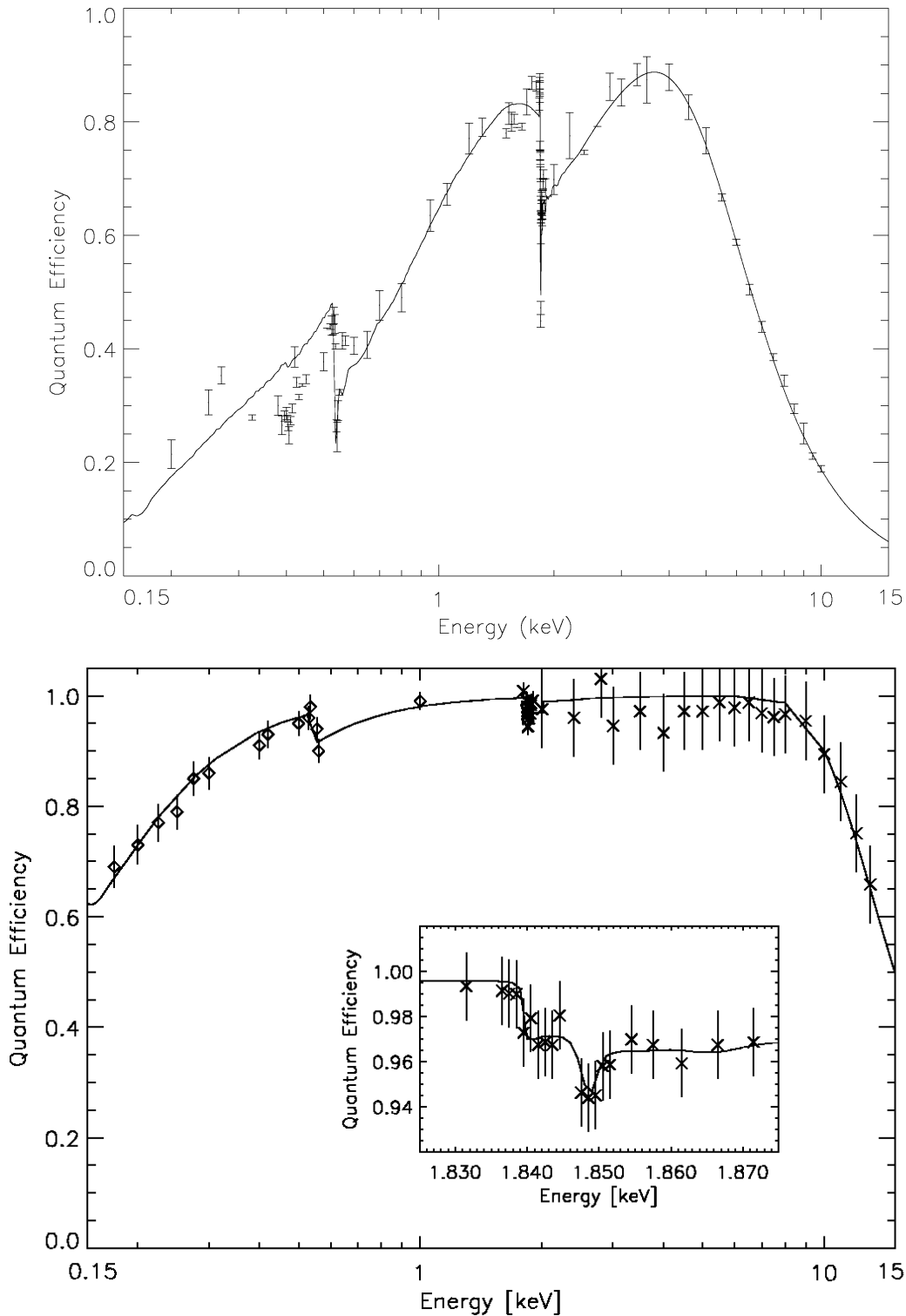
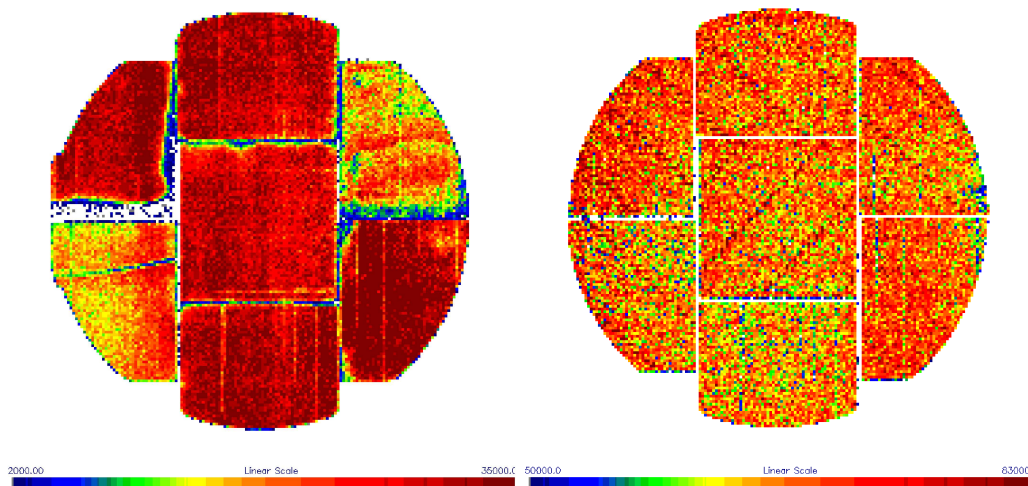


Figure 1-8:QE ground measurements and CCF (upper MOS1 CCD1, lower PN)



**Figure 1-9:**  
**QE spatial inhomogeneities within MOS1 appearing only at very low energies**  
**(left 150 eV, right 400 eV). The regularly spaced "hot pixels" seen in the 400 eV image are not hot pixels at all,**  
**they have been interpreted as false events generated by the reset-on-demand mechanism.**

#### 1.2.4 Vignetting

Vignetting means: reduction in the effective area with radial distance from the telescope's axis.

The telescope vignetting is [well determined for off-axis angles of up to more than 10'](#).

One of the most important outstanding problems of the calibration was an offset of around 1' in the telescope axis from nominal. This did not affect the astrometry but could have been the reason for some of the flux discrepancies between MOS and PN caused by the vignetting correction which has not yet been adapted to this offset in SAS versions earlier than 6.0.0. The offset was determined and implemented in the corresponding CCF (XMM\_MISCDATA\_0020). With SAS 6.0.0 and the current available CCF the new consideration of the right optical axis position improves the vignetting correction. However the vignetting correction itself has not changed at all, the only difference is, that it is now applied for correct off axis angles, that could not be calculated correctly before due to the wrong information for the optical axis. This improves differences in flux for off axis sources for each camera from  $\pm 14\%$  to  $\pm 5\%$ . Detailed information can be found in XMM-CAL-TN-54 and XMM-CAL-SRN-0156.

XMM-SOC-CAL-TN-0018

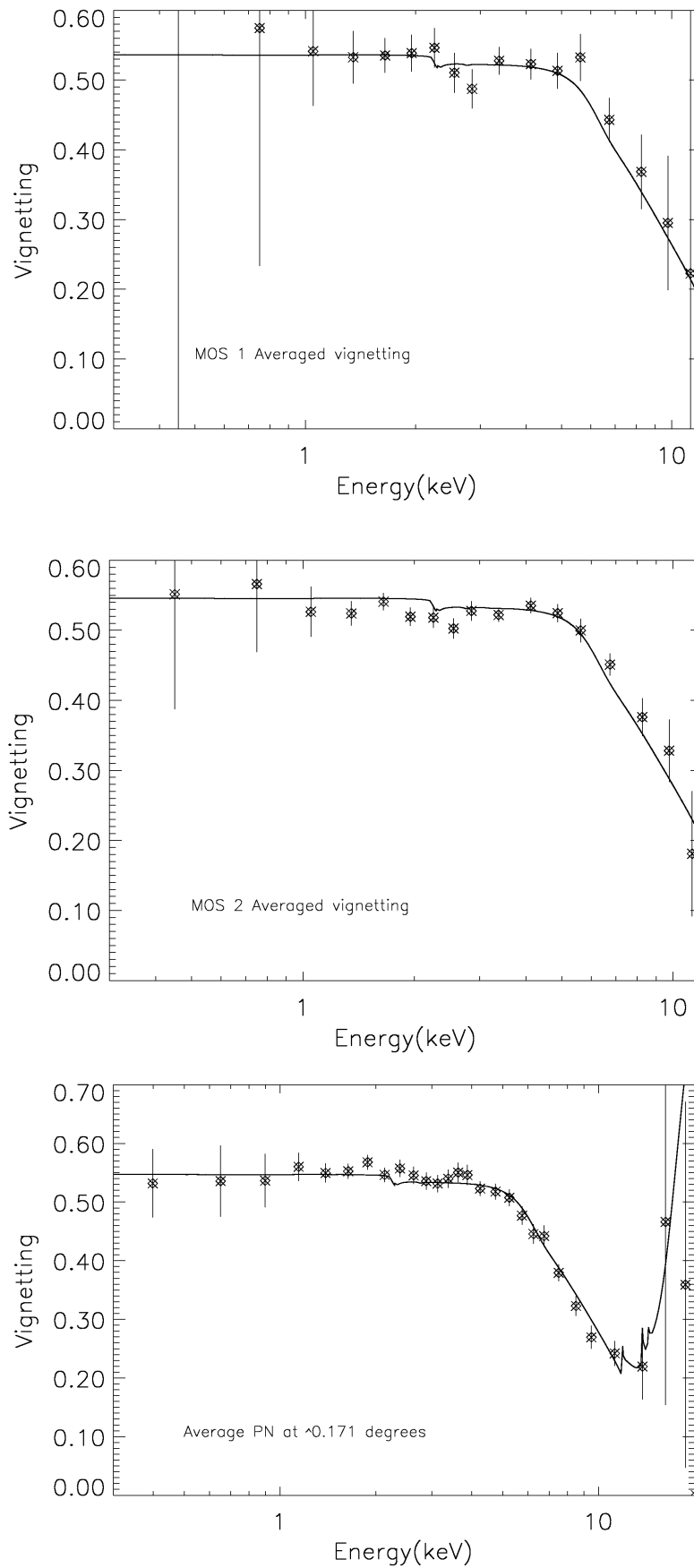


**Figure 1-10: Average vignetting measured over 4 azimuths at an off-axis angle of around 10's derived from Calibration measurements of the SNR G21.5-09**

### 1.3 Energy Redistribution

Energy Redistribution means: The energy profile recorded by the detector system in response to a monochromatic input.

#### 1.3.1 MOS

The same energy redistribution matrices can be used for all MOS imaging modes. Since SAS 5.4.1, *rmfgen* supports all MOS modes and takes the observed change in energy resolution with time into account. Also ready-made redistribution matrices, addressing this, are available at [http://xmm.vilspa.esa.es/external/xmm\\_sw\\_cal/calib/epic\\_files.shtml](http://xmm.vilspa.esa.es/external/xmm_sw_cal/calib/epic_files.shtml).

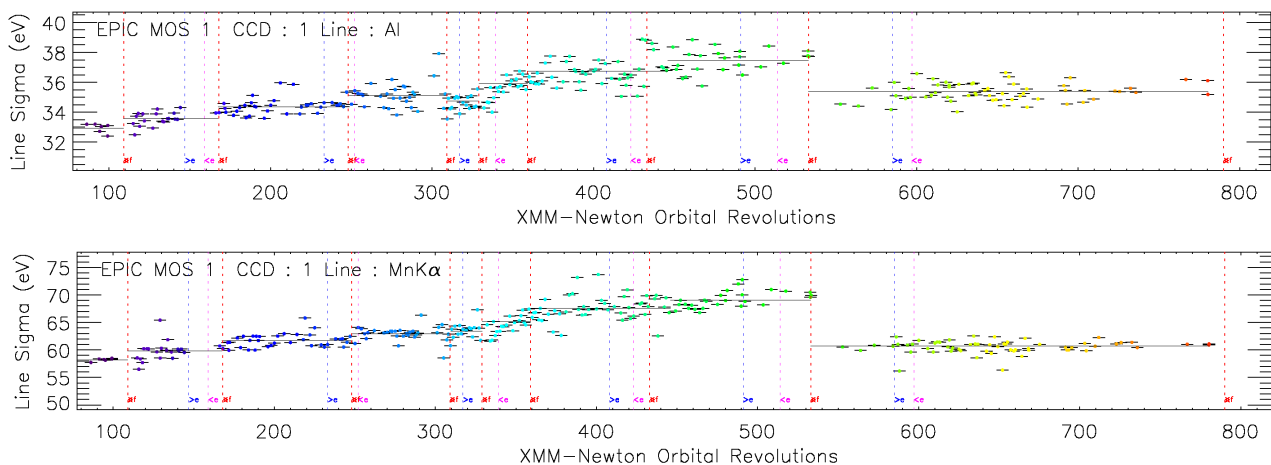


**Figure 1-11:**  
Energy resolution MOS 1 CCD1 in eV. The drop after rev 532 is caused by the cooling of the cameras

#### 1.3.2 PN

The energy redistribution is mode dependent for the PN camera. That means that different response matrices are needed for the different modes. Since SAS 5.4.1 *rmfgen* supports all modes. Also ready-made matrices can be used, which can be obtained at:

[http://xmm.vilspa.esa.es/external/xmm\\_sw\\_cal/calib/epic\\_files.shtml](http://xmm.vilspa.esa.es/external/xmm_sw_cal/calib/epic_files.shtml).

The response is mainly studied for on-axis sources. The response matrices are for all CCDs (note that for SW, TIMING and BURST only the CCD containing the focal point is used); the only dependence of the redistribution (i.e. the energy resolution) is the RAWY dependence (see 2.2.2). Other off-axis (radial) dependencies do not exist in the re-distribution, vignetting is part of the effective areas computed by *arfgn*.

More information on *rmfgen* and *arfgn* are available at:

<http://xmm.vilspa.esa.es/sas/current/doc/arfgn/index.html>

<http://xmm.vilspa.esa.es/sas/current/doc/rmfgen/index.html>.

We do not see any significant degradation of energy resolution with time in PN.

EPIC-pn spectra from Zeta Puppis have shown that the spectral response below about 400 eV is not yet correctly reproduced. In particular the re-distribution as modelled in SAS 6.0.0 is higher than seen in the data. This can lead to large (30%) systematic errors in the absolute flux of very soft spectral components ( $kT < 100$  eV). Further observations with different read-out modes are planned to investigate the problem.

### 1.4 CTI/Gain

CTI means: Charge Transfer Inefficiency is the imperfect transfer of charge as it is transported through the CCD to the output amplifiers during read-out.

Gain means: Gain is the conversion (amplification) of the charge signal deposited by a detected photon, from ADU (Analogue to digital unit) charge into energy (electron-volts).

For the instruments in normal conditions, the Gain and CTI are known well enough such that **the line energy can be determined with an uncertainty of 5 eV over the full energy range for all MOS imaging modes and with an uncertainty of 10 eV over the full energy range for all pn imaging modes except pn Extended Full Frame where for the internal calibration source an over correction of up to 15 eV can be seen.** This is currently under investigation with special calibration observations. An improvement in the epoch dependent CTI and Gain correction in SAS 6.0.0 has reduced the uncertainty from 10 to 5 eV for the MOS cameras. Abnormal conditions include the eclipse seasons and solar flares (marked by the vertical lines in figures 1-11, 1-12), where the gain at the beginning of an orbit (i.e. during calibration observations) can vary significantly from the gain for the remainder of the orbit, due to temperature variations in the on-board electronics. No correction has been achieved yet for this, but the effect of the EMAE (EPIC MOS Analogue Electronics) temperature excursions during scientific observations are usually small (MOS1: < 10eV at Mn-K and < 5eV at Al-K).

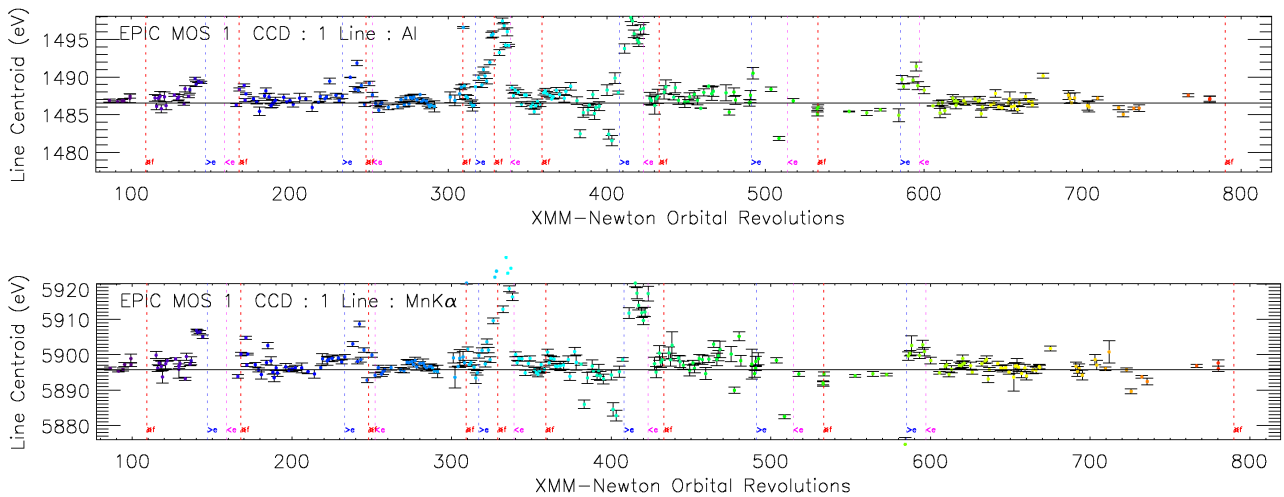


**Figure 1-12: MOS 1 CCD 1 Calibration source line positions at Al-K (upper) Mn-K (lower)**

The **relative accuracy of the Timing modes compared to the imaging modes is better than 0.3 % over the full energy range.**

For the PN, deviations in the gain occurred during the first eclipse season (revolutions 60-80) and during occasions when the RGS was first turned off to diagnose a CCD chain failure (revolutions 136-146, and 149-150), when the platform temperature changed significantly and 10 - 30 eV discrepancies were occasionally observed. The PN team has established a good correlation to implement a temperature dependent gain correction, which is already implemented in the SAS, but not yet activated, since full consequences of the correction have not yet fully been investigated. The feature however is currently regarded as low priority. Fortunately the temperature excursions are now dramatically reduced.

Revolution	Problem
60 – 80	1 <sup>st</sup> Eclipse
136-146	RGS off
149-150	RGS off

Note: For PN a lower temperature means a lower gain (too low energies) while for MOS it is vice versa ( $\Delta\text{gain(PN)}/\Delta T > 0$ ,  $\Delta\text{gain(MOS)}/\Delta T < 0$ )

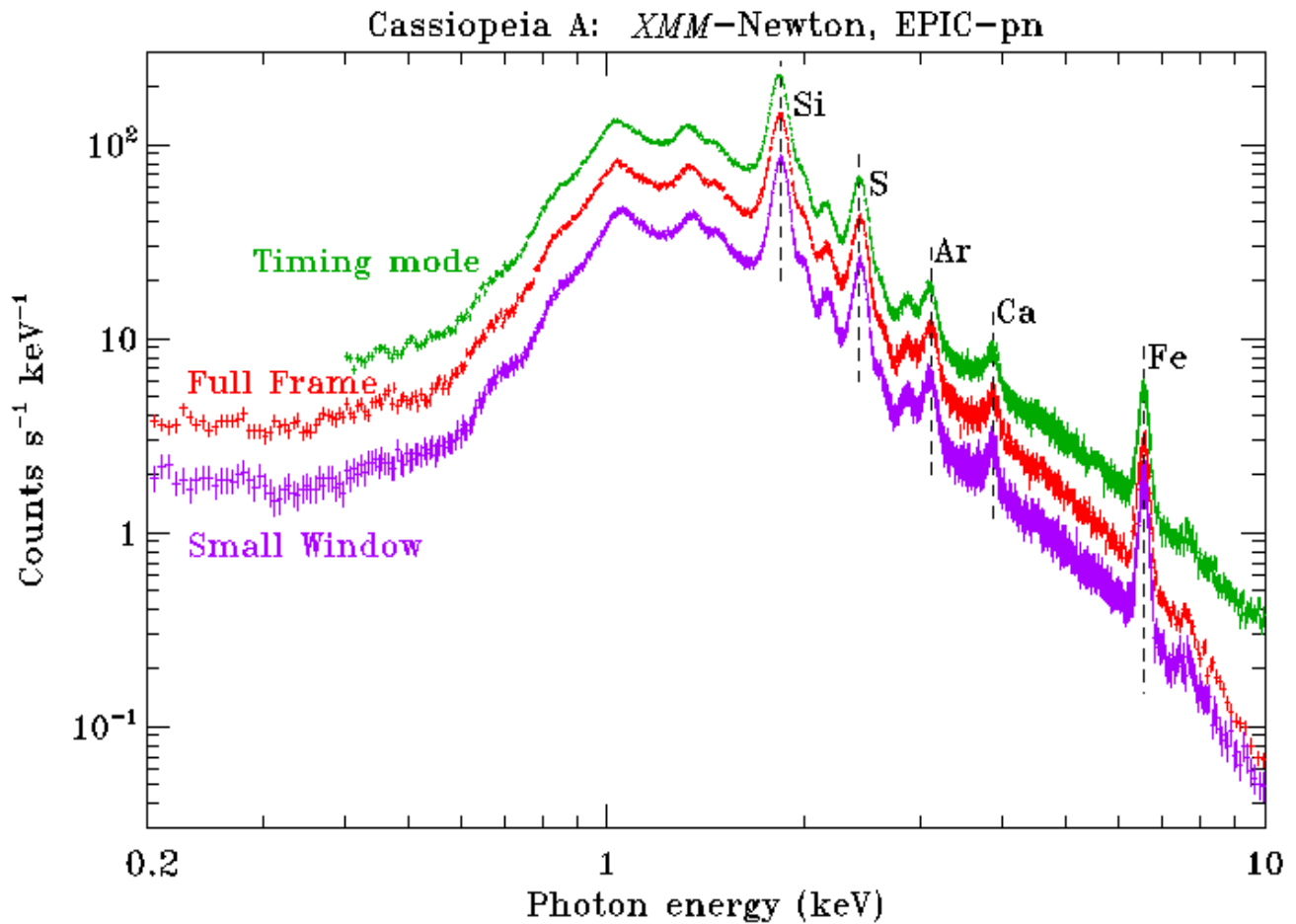


Figure 1-13: Cas-A spectra in different PN-Modes  
 (count rate spectra are scaled for clarity)

## 1.5 Background

There are three different types of background:

1. The astrophysical background dominated by thermal emission at lower energies ( $E < 1$  keV) and a power law at higher energies (primarily from unresolved cosmological sources). This background varies over the sky at lower energies.
2. Soft proton flares where the spectrum varies from flare to flare. For weak sources the only option is to select quiet time periods from the data stream for analysis. To identify intervals of flaring background the observer should generate a light curve of high energy ( $E > 10$  keV) single pixel (PATTERN = 0) events. To identify good time intervals use the selection criteria:
  - MOS:  $< 0.35$  cts/s (#XMMEA\_EM && (PI>10000) && (PATTERN==0) on the full FOV
  - PN:  $< 1.0$  cts/s (#XMMEA\_EP && (PI>10000) && (PATTERN==0) on the full FOV

Note: These selection criteria assume that sources above 10 keV do not contribute significantly to the overall intensity.

- The high-energy proton induced background. These events are created directly by the protons penetrating the CCDs and indirectly by the fluorescence of satellite material to which the detectors are exposed. This background is being actively investigated and there are two samples of blank sky high galactic latitude background event files available at [http://xmm.vilspa.esa.es/external/xmm\\_sw\\_cal/calib/epic\\_files.shtml](http://xmm.vilspa.esa.es/external/xmm_sw_cal/calib/epic_files.shtml) for use as templates. The goal is to provide a generic-modelling tool for all observation scenarios.

The following two images show the strong metal line features that make the background subtraction complex, especially for large clusters and radial temperature determination.

Explanatory notes for background subtraction are given:

[http://xmm.vilspa.esa.es/external/xmm\\_sw\\_cal/calib/epic\\_files.shtml](http://xmm.vilspa.esa.es/external/xmm_sw_cal/calib/epic_files.shtml).

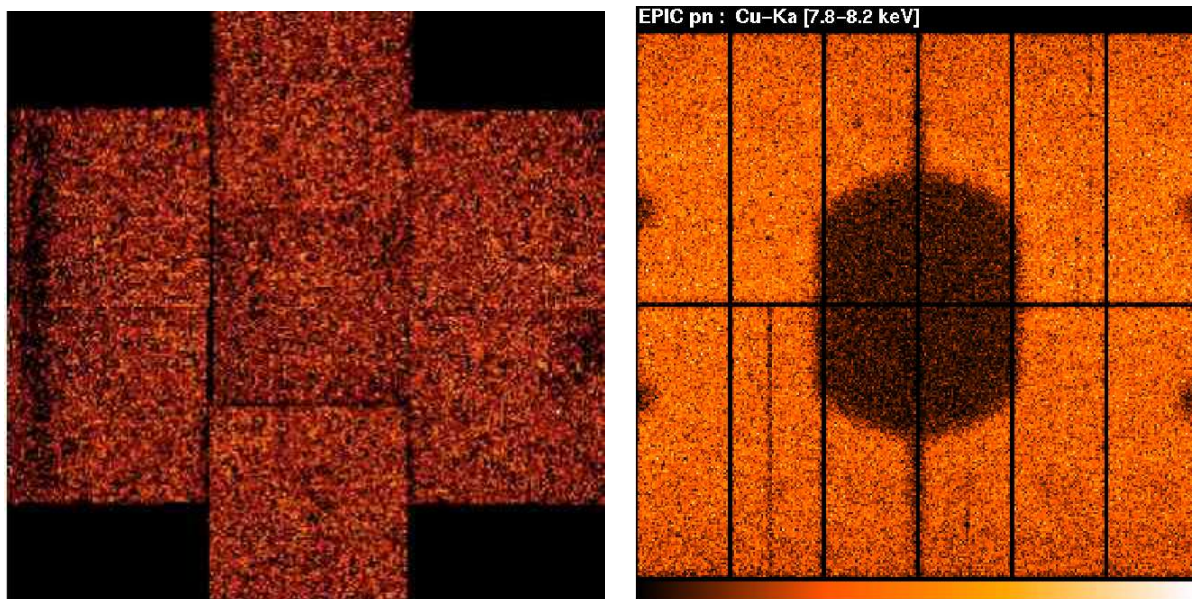


**Figure 1-14: MOS-Al-K at 1.48 keV (left) and PN Cu-K at 8.04 keV (right) internal background caused by X-ray fluorescence lines correlated with the structures of the electronic board (pn-Cu-K) and the more distant camera itself (MOS Al-K)**

## 1.6 Timing

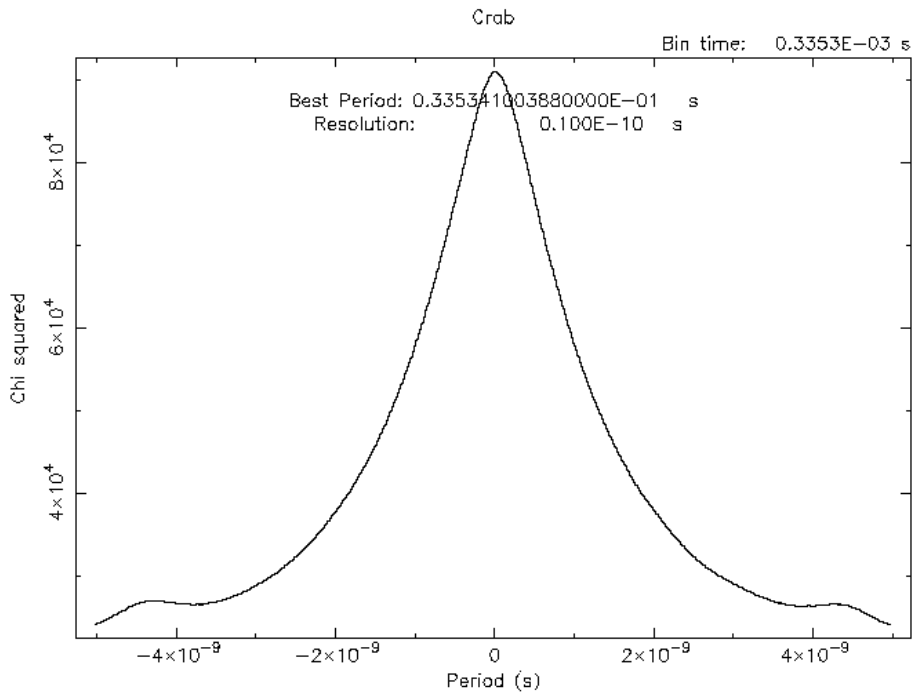
Absolute timing means: Locating events in time with reference to standard time defined by atomic clocks or other satellites.

Relative timing means: The capacity to measure time intervals and periodicity reliably

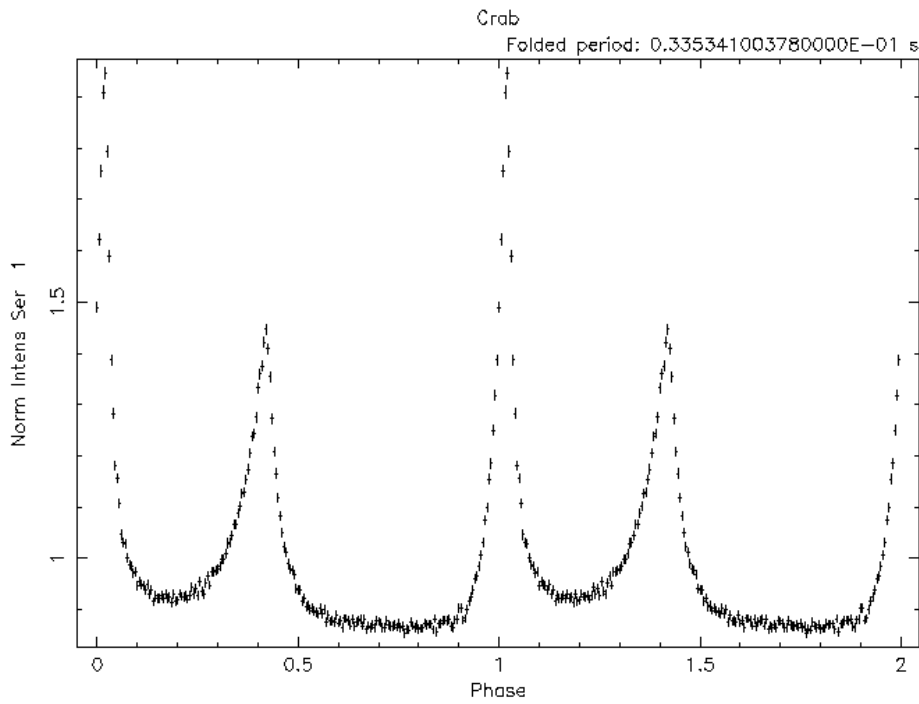
The release of SAS 5.3.3 included for the first time all necessary components to support timing analysis with outstanding time resolutions down to 29 and 7 microseconds for PN Timing and Burst modes respectively. Tests on data from the Crab pulsar taken during XMM-Newton's performance verification campaign in early 2000 indicate that the **relative deviation in the observed pulse period w.r.t. the most accurate radio data available ( $\Delta P/P$ ) is now considerably less than  $10^{-8}$** , with an **absolute timing accuracy of  $< 500$  microseconds**.

For the Crab pulsar the new results now conform with estimates of the theoretically attainable accuracy with XMM-Newton and the expected statistical errors. Further investigations of periodicity of other objects are currently underway.

Because of another improvement in converting the *onboard time* (running counter, kept by the CDMU and synchronised with all the Data Handling units. 48 bits, resolution (LSbit) is 1/65536 secs) to the *event time* (time in a counter internal to the EPEA that timestamps each frame. This timer is reset to 0 at the beginning of each observation, at a sharp (integer) second of OBT), the user should make sure that the data are fully reprocessed with the SAS higher than SAS 5.3.3 and not only with the new "barycen" task of SAS 5.3.3 in order to achieve the highest timing accuracy.



Start Time 0 0: 0: 0: 0 Stop Time 0 0: 0: 0: 0



Start Time 12340 16:22:49:177 Stop Time 12341 22:42:39:295

Figure 1-15:  $\chi^2$ -distribution of epoch folding period search (upper) folded light curve for the Crab

## 1.7 Examples of EPIC spectra

This section gives only two examples of spectra, since we will publish in the near future a special document of XMM-Newton Cross Calibration, that will in detail elaborate the current status of XMM-Cross-Calibration.

### 1.7.1 PKS 0558-508

This section presents a comparison of EPIC results for the radio-loud narrow-line Seyfert 1 galaxy PKS0558-508.

Figure 1-17 shows the simultaneous fits to EPIC data where the only independent parameter was a scale factor between the different instruments. The refined PSF correction brings now a much better agreement for the three cameras for that overall normalization. Whereas in previous versions the EPIC cameras agreed within  $\pm 10-12\%$  in that overall normalisation we see now more values like  $\pm 5\%$ . For details see XMM-SOC-CAL-TN-0052 (to be released soon).

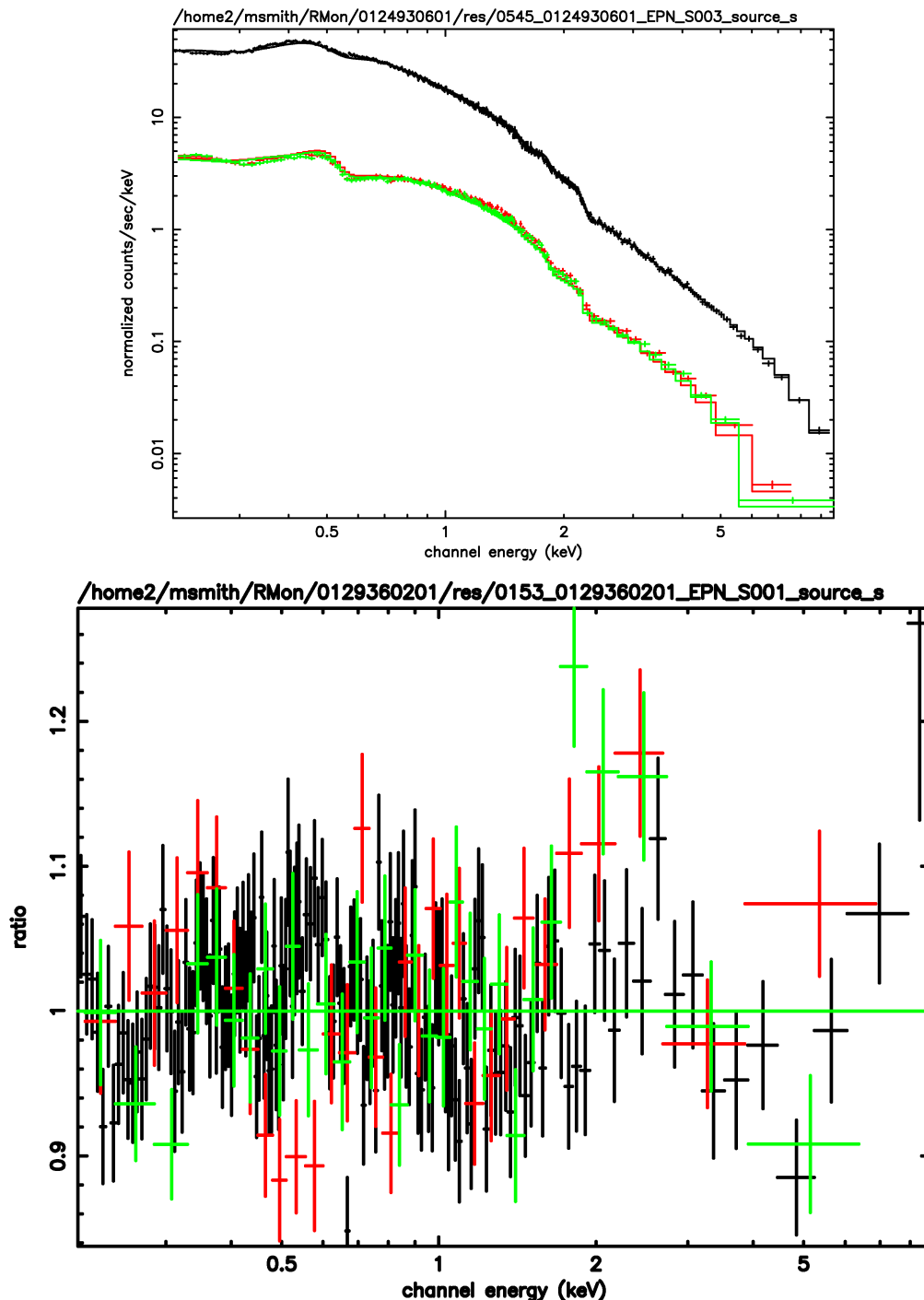


Figure 1-16: Simultaneous spectral fits to PKS0558-508. Black: pn, red, MOS1, green: MOS2. The zoomed ratio (lower panel) has been binned more for clarity.

### 1.7.2 PKS 2155-304

The following plot shows a simultaneous fits to EPIC PKS2155-304 data where the only independent parameter was a scale factor between the different instruments. Also her the new PSF correction improved the overall normalization from  $\pm 10-12\%$  to  $\pm 5\%$ . The larger residuals below 600 eV are due to uncertainties arising from the complicated shape of the redistribution function and the low energy effective area in combination with a gain problem of the pn-SW mode, that is currently under investigation. Above 7 keV the residuals probably arise form uncertainties in the background subtraction method.

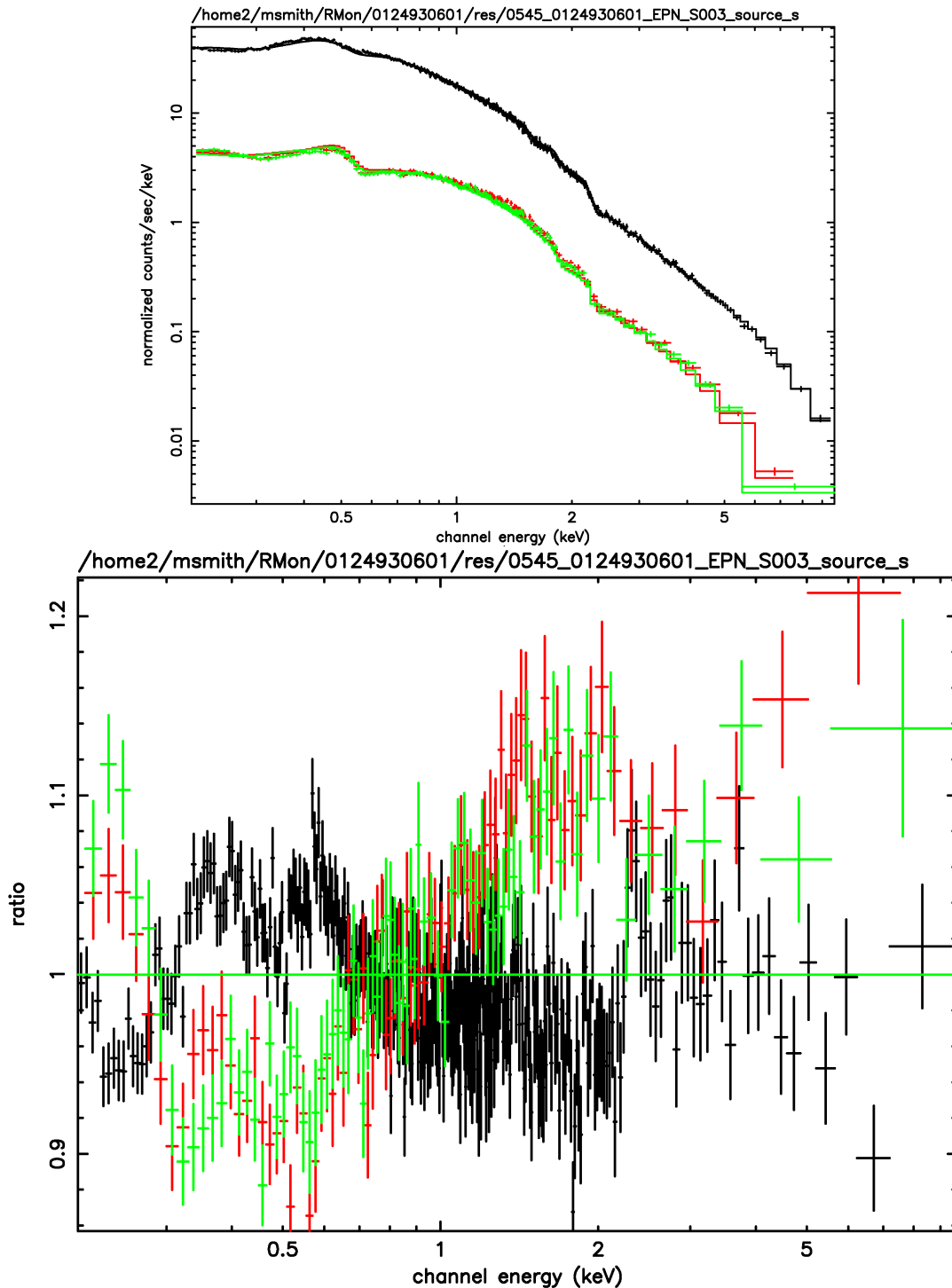


Figure 1-17: Simultaneous spectral fits to PKS2155-304. Black: pn, red, MOS1, green: MOS2. The zoomed ratio (lower panel) has been binned more for clarity.

## 1.8 Cross Calibration with RGS and other Satellites

These sections have been removed since in the near future a dedicated Cross Calibration Document will be available at the XMM-Newton Science Operations Center web portal.

## 2 Data Analysis

This section provides an overview of what the SAS is able to do with the V6.0.0 release. Also included is a guideline of how to work with the different modes of the cameras.

### 2.1 New features in SAS

#### 2.1.1 SAS 5.3.0

- The MOS CTI correction has been improved to take into account the changes which have occurred since launch.
- A new task, *evigweight*, assigns a vignetting correction to each individual event. This allows extraction of vignetting-corrected images and spectra directly.
- A new task, *epatplot*, is available to identify pile up.
- The PN background rejection and CTI correction have been significantly improved.
- The tasks *rmfgen* and *arfgen* now reproduce the canned matrices to within 1%. Also, the full range of event patterns is supported. Further, *rmfgen* supports the major observing modes.

#### 2.1.2 SAS 5.3.3

- The latest CTI correction for PN SW and LW mode has been implemented.
- EPIC-PN Timing and Burst mode response files are available

#### 2.1.3 SAS 5.4.1

- MOS CTI correction has been modified in order to compensate the stepwise degradation after solar flares
- Degradation of the MOS intrinsic spectral resolution due to the larger noise component of the degraded CTI has been modelled.
- Refined calculation of the MOS gain as a function of observation epoch has been implemented.
- *epatplot* now also indicates the distribution and amount of invalid PN patterns to ease flux comparison in the case of pattern pile-up.
- New PN quantum efficiency function which is based on measurements of the thickness of the SiO<sub>2</sub> layer on top of the CCD.

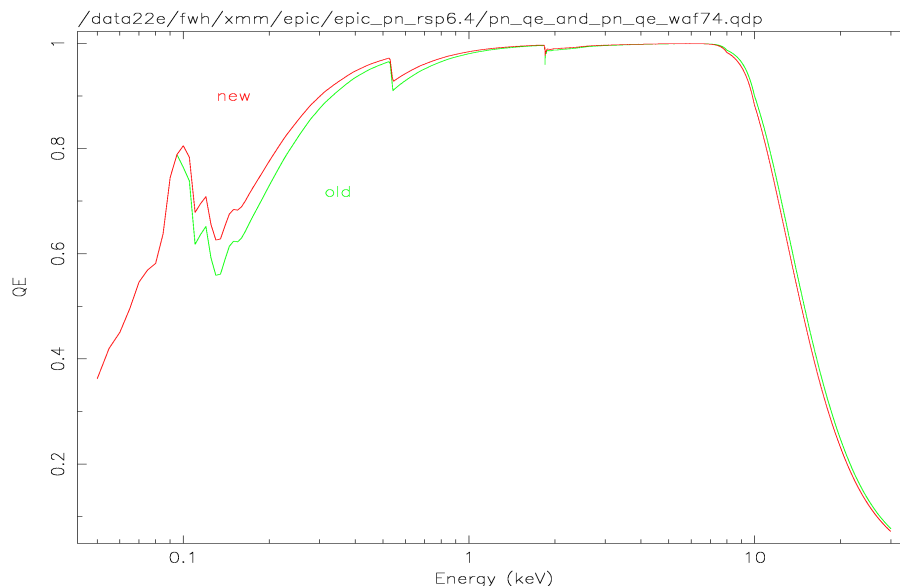


Figure 2-1: New (red) and old (green) PN QE

- Refined spectral redistribution for PN (concerns all readout modes) at energies below 600 eV. The redistribution was adjusted to achieve agreement in column density derived from PN and Chandra LETG spectra of RXJ1856.3-3754.
- *calpnalgo* now receives all quantities from CCFs.
- The SW/LW mode CTI-correction function for PN has been modified.
- *arfgen* and *rmfgen* now support all modes (incl. TI and BU modes).

#### 2.1.4 SAS 6.0.0

- The new SAS task *epreject* corrects shifts in the energy scale of specific pixels due to high-energy particles hitting the EPIC PN detector during offset map calculation and suppresses the detector noise at low energies by statistically flagging events based on the known noise properties of the lowest energy channels. In the case of timing mode data, flagging of soft flare events may be performed.
- An additional function is added to *emevents* that performs a blanking of bad-energy columns and handles those now correctly as dead areas.
- *emevents* is now doing a filtering & removal of flickering pixels decreasing significantly the noise at low-energies.
- The new SAS tasks *ebadpixupdate* allows operations on bad pixels at the level of the calibrated events list
- *epatplot*: The optional input of a background eventset now allows the determination of background-subtracted pattern fractions. This is useful, e.g., in the case of extended source analysis or close to spectral background features.
- *badpixfind*: The task now permits bad pixel searching on calibrated multi-chip (i.e. final pipeline product) eventsets. Previous versions only operated on raw event sets.

## 2.2 Data Analysis

In the next section some general recommendations for conservative data analysis are provided.

This includes:

- Where should data be taken from the CCD
- Which energy range should be used
- Which pattern range should be used
- Which response matrix should be used

For detailed guidelines of XMM data analysis please use the SAS Users' Guide at

[http://xmm.vilspa.esa.es/external/xmm\\_sw\\_cal/sas\\_frame.shtml](http://xmm.vilspa.esa.es/external/xmm_sw_cal/sas_frame.shtml)

### 2.2.1 MOS

#### Imaging modes

**Source region:** where appropriate

**Background region:**

- point source - From the same observation another region of the same area off-axis, away from source counts.
- extended source - This is more complicated. Please have a look at explanatory notes available on the XMM web site at <http://xmm.vilspa.esa.es/ccf/epic/#background>.

**Energy range:** 0.2-10.0 keV (However, because of calibration uncertainties, care must be taken when interpreting data below 0.3 keV.)

In general the user should use [patterns](#) 0-12. (see XMM Users Handbook section 3.3.10 available at [http://xmm.vilspa.esa.es/external/xmm\\_user\\_support/documentation/index.shtml](http://xmm.vilspa.esa.es/external/xmm_user_support/documentation/index.shtml)). However, pattern 0 events can be used to minimise the effects (e.g. spectral distortion) of pile-up. Pattern 0 events can also be used for observations in which the best-possible spectral resolution is crucial and the corresponding loss of counts is not important. In addition the user should only use events flagged as “good” by using (#XMMEA\_EM) in the selection expression window of *xmmselect*. When analysing spectra the user should use arf files produced by the SAS (version 5.3.0 or above) task *arfgen* in conjunction with canned redistribution matrices or produce those with the SAS task *rmfgen*.

### Timing modes

**Source region:** where appropriate

**Background region:** background subtraction will not usually be an issue for sources observed in timing mode. However because the timing strip is only 100 pixels wide background regions should be taken from the outer CCDs.

**Energy range:** 0.3-10.0 keV

**Pattern** 0 only.

As for imaging mode, canned redistribution matrices valid for timing mode will be made available and should be used with arf files produced by the SAS.

### 2.2.2 PN

#### Imaging modes

**Source region:** where appropriate

**Background region:**

- point source - From the same observation but away from source. Ideally the region should have the same distance to the readout node (RAWY) as the source region. This ensures that similar low-energy noise is subtracted, because it increases towards the readout-node. Do not use the columns passing the source to avoid out-of-time events from the source, i.e. do not use an annulus around the source region.
- extended source - see 2.2.1

**Energy range:** 0.15 keV - 15 keV, however both limits depend on readout mode and aim of the analysis.

For imaging purposes [pattern](#) 0-12 can in principle be used.

Since doubles (1-4), triples (5-8) and quadruples (9-12) (see XMM Users Handbook section 3.3.10 available at [http://xmm.vilspa.esa.es/external/xmm\\_user\\_support/documentation/index.shtml](http://xmm.vilspa.esa.es/external/xmm_user_support/documentation/index.shtml)) are only created above twice, three and four times the low-energy threshold, respectively, cleanest images are produced by excluding the energy range just above the thresholds. E.g. to produce a 0.2 - 10 keV image one may select singles from the whole energy band and doubles only from 0.4 keV. FLAG == 0 omits parts of the detector area like border pixels, columns with higher offset, etc. This may be not desired (and is unnecessary) in the case of broad-band images.

For spectral analysis, response matrices are available only for singles, doubles and singles+doubles. Higher order pattern types are of low statistical significance, have degraded spectral resolution and are therefore not useful. Best spectral resolution is reached by selecting singles for the spectrum. FLAG == 0 should be used for high accuracy to exclude border pixels (and columns with higher offset) for which the pattern type and the total energy is known with significantly lower precision. At high energies the fraction of doubles is however almost as high as that of singles and to include doubles is recommended to increase the statistics. If a sufficient number of counts is available single- and double-spectra can be created separately and fitted simultaneously in XSPEC (with all parameters including *norm* linked together). One exception is the timing mode (see below).

To choose the valid energy band for the spectral fit it is highly recommended to use the task *epatplot*. It uses as input a spatially selected (source region) event file and plots the fractions of the various patterns as function of energy. Spectral analysis should only be done in the energy band(s) where single- (and double-) fractions match the expected curves. In some observations the low-energy noise can be high, restricting the useful band at low energies. Deviations at medium energies indicate pile-up (more doubles than expected) and in such cases the inner part of the PSF in the source region

should be excluded for spectral analysis. (More information on that topic is available in the XMM Users Handbook at [http://xmm.vilspa.esa.es/external/xmm\\_user\\_support/documentation/index.shtml](http://xmm.vilspa.esa.es/external/xmm_user_support/documentation/index.shtml)).

The user should use arf files produced by the SAS (version 5.3.3 or above) task *arfgen* in conjunction with canned redistribution matrices (which are compatible to the CTI correction used in 5.3.3 or above) or produce those with the SAS task *rmfgen*. For each readout mode of the PN a set of rmf files is available (for singles, doubles, singles+doubles. Except timing mode where only singles+doubles must be used). The CTI causes a dependence of spectral resolution with distance to the readout node. Therefore the 200 lines of each CCD are divided into areas of 20 lines each (Y0 at readout, Y9 at opposite side, which includes the nominal focus point) and for each area an rmf file is available

### Timing and Burst modes

**Source region:** Columns around source position

**Background region:** Columns away from source

The RAWY coordinate is related to a fine-time, selection on RAWY will therefore exclude certain time periods. For timing mode no such selection on RAWY is recommended; in burst mode use  $RAWY < 160$  to avoid direct illumination by the source. For timing mode only singles+doubles should be selected for a spectrum and the fit restricted to energies  $> 0.5$  keV to avoid the increased noise. For burst mode energies  $> 0.4$  keV can be used with combinations of singles/doubles as in the window modes.